Materials Transactions, Vol. 64, No. 4 (2023) pp. 877 to 884

Stabilization of Equiatomic Solutions Due to High-Entropy Effect

Taichi Abe[1,*], Kwangsik Han[1], Yumi Goto[1], Ikuo Ohnuma[1] and Toshiyuki Koyama[2]

[1]*National Institute for Materials Science, Tsukuba 305-0047, Japan*
[2]*Nagoya University, Nagoya 464-8601, Japan*

The stability of solid-solution phases in FCC and BCC lattices was examined in multi-component alloys based on the CALPHAD technique using the compound energy formalism and regular solution model. From the thermodynamic calculations, it was found in ternary systems that the single solid-solution phase became stable around the equiatomic composition where the configurational entropy was the largest value. The transition temperature from the disordered phase to ordered phase(s) or miscibility gap(s) decreased with the increasing number of elements in the system. The order-disorder transition temperature on the FCC lattice was affected by the end member of the ordered phases existing at the equiatomic composition, whereas it was not significant for the order-disorder transition in the BCC lattice. The single solid-solution phase region at equiatomic compositions was affected by variations in the interaction parameters. In multi-component systems, the variations were averaged with increasing the number of elements in the system. This suggests that high-entropy alloys can afford a variety of elements. This study shows that the disordered state can be formed in multicomponent systems around the equiatomic composition and suggests clearly that due to the high-entropy effect, the solution phases are stabilized. [doi:10.2320/matertrans.MT-M2022167]

(Received October 19, 2022; Accepted January 16, 2023; Published February 3, 2023)

Keywords: *regular solution, order-disorder transition, phase stability, miscibility gap*

1. Introduction

High-entropy alloys (HEAs)[1)] have been intensively investigated and synthesized in various alloy systems with face-centered cubic (FCC),[2–5)] body-centered cubic (BCC),[6,7)] and hexagonal close-packed (HCP) structures.[8)] HEAs are defined based on the configurational entropy, S^{conf}, in the Bragg-Williams-Gorsky (B-W-G) approximation, which is given by $S^{\mathrm{conf}} = -R\sum x_i \ln x_i$, where R is the gas constant and x_i is the mole fraction of element i. By mixing multiple elements, S^{conf} increases and becomes "high" in HEAs. The S^{conf} of equiatomic alloys with five elements is $R\ln 5 \simeq 1.61R$, which is used as a guiding value for HEAs. This concept has been expanded to lower entropy alloys, such as medium-entropy alloys (MEAs) with $0.69R < S^{\mathrm{conf}} < 1.61R$ and low-entropy alloys with $S^{\mathrm{conf}} < 0.69R = R\ln 2$. According to the narrow definition of HEAs, the microstructure of these alloys consists of a single solid-solution phase. However, in many HEAs, microstructures include second phases such as intermetallic compounds or other solution phases. As the co-existence of the second phases changes the S^{conf} of the matrix phase, they may affect the mechanical properties of HEAs.[9)] For the formation of HEAs, Yang and Zhang[10)] proposed two parameters: Ω, which is related to the mixing quantity and δ, which is related to the size misfits between atoms. They found that HEAs can form in the region where $\Omega \geq 1.1$ and $\delta \geq 6.6\%$. Based on phase diagrams, the existence of a single solid-solution phase region is prevented by the formation of i) intermetallic compounds, ii) miscibility gaps, or iii) other solid-solution phases. Although Takeuchi *et al.*[8,11–13)] examined the stability of solution phases based on the valence electron concentration (VEC), the stability of solution phases with respect to intermetallic compounds and miscibility gaps has not yet been discussed. Therefore, the purpose of this study was to examine the relative stability of single-phase HEAs with FCC or BCC structures in the formation of compounds and miscibility gaps based on the CALPHAD (CALculations of PHAse Diagrams) technique.[14)]

*Corresponding author, E-mail: abe.taichi@nims.go.jp

2. Gibbs Energy Functions

2.1 Gibbs energy of solution phases

The Gibbs energy of the solution phases, $G_{\mathrm{m}}^{\mathrm{dis}}$, is described by the substitutional solution model[14)] as follows:

$$G^{\mathrm{dis}} = \sum x_i {}^0G_i^{\mathrm{dis}} + RT\sum x_i \ln x_i + G^{\mathrm{excess}} \quad (1)$$

where ${}^0G_i^{\mathrm{dis}}$ and T are the Gibbs energy of a pure element i and the temperature in Kelvin, respectively. The third term on the right-hand side, G^{excess}, is the excess Gibbs energy given by the Redlich-Kister (R-K) polynomial as follows:

$$G^{\mathrm{excess}} = \sum_{i,j} x_i x_j \sum_{v=0} L_{i,j}^{(v)}(x_i - x_j)^v \quad (2)$$

where $L_{i,j}^{(v)}$ is the v-th R-K parameter between elements i and j. When $L_{i,j}^{(v)} = 0$ (except $L_{i,j}^{(0)} \neq 0$), this solution is called the regular solution. When $L_{i,j}^{(0)} < 0$ (attractive interaction between i and j), the solution phases can have miscibility gaps[15)] at low temperatures, while when $L_{i,j}^{(0)} > 0$, ordered phases are formed instead of miscibility gaps. For the ideal solution, the excess Gibbs energy term of eq. (1) is zero ($G^{\mathrm{excess}} = 0$). For equiatomic n-component alloys, where $x_i = 1/n$, eq. (2) can be simply written as:

$$G^{\mathrm{excess}} = \frac{1}{n^2}\sum_{i,j} L_{i,j}^{(0)}. \quad (3)$$

By using a pair interaction energy, $w_{i,j}$, eq. (3) can be written as:

$$G^{\mathrm{excess}} = \frac{z}{n^2}\sum_{i,j} w_{i,j} \quad (4)$$

where z is the coordination number in the nearest-neighbor shell, and is equal to 12 and 8 for the FCC and BCC phases, respectively. A negative value of the parameter ($w_{i,j} < 0$) indicates an attractive interaction between the i and j atoms, whereas a positive value indicates a repulsive interaction

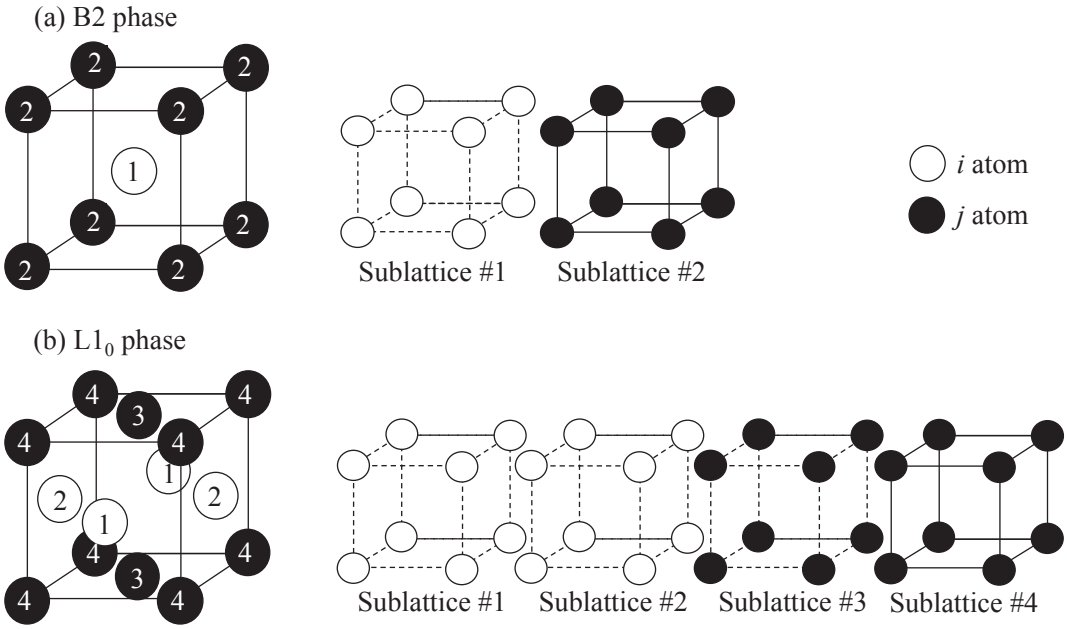

Fig. 1 (a) Four equivalent sublattices for the FCC lattice in the $L1_0$ phase, where #1=#2≠#3=#4, and (b) two equivalent sublattices for the BCC lattice in the B2 phase, where #1≠#2 in the *i-j* binary system.

between the *i* and *j* atoms. In the following calculations, the $\sum x_i{}^0G_i^{\mathrm{dis}}$ term in eq. (1) is zero because the Gibbs energy of pure elements is considered as the reference state. Only binary interactions were considered for the excess Gibbs energy term.

2.2 Gibbs energy of BCC-based phases with two sublattices

The B2 ordered phase and A2 disordered phase were modeled using the two-sublattice model. The sublattice configuration of the B2 phase is illustrated in Fig. 1(a). It is selected in such a way that all sublattices are equivalent and have an equal number of sites and bonds to the other sublattices. The Gibbs energy equation for the two-sublattice phase in an *i-j* binary system using the compound energy formalism (CEF)[16] is

$$G^{2\mathrm{sl}} = \sum_{i,j} y_i^{(1)} y_j^{(2)} G_{i:j} + RT\frac{1}{2}\sum_{m=1}^{2}\sum_{i} y_i^{(m)} \ln y_i^{(m)} \quad (5)$$

where $G_{i:j}$ is the Gibbs energy of the *i*:*j* compound. A colon in the suffix of the Gibbs energies separates elements on different sublattices and a comma separates elements on the same sublattice. In the two-sublattice model, the sublattices are numbered as #1 and #2 from left to right in the suffix. For example, *i*:*j* stands for *i* on the sublattice#1 and *j* on the sublattice#2. By counting the number of the unlike pairs, the Gibbs energies of the end members are given by $G_{i:j} = G_{j:i} = 4w_{i,j}$ and $G_{i:i} = G_{j:j} = 0$.

To simplify the integration of an ordered BCC phase with a database where many systems have BCC phases without any orderings, it is advantageous to partition the Gibbs energy of an ordered phase into two parts (eq. (6)), as follows:

$$G^{\mathrm{ord}} = G^{\mathrm{dis}}(\{x_i\}) + \Delta G^{\mathrm{ord}}(\{y_i^{(m)}\}) \quad (6)$$

where $\{x_i\}$ and $\{y_i^{(m)}\}$ denote the mole fraction and the site fraction of all independent components. When the ordered phase is disordered, the second term on the right side of eq. (6) becomes zero, i.e., $\Delta G^{\mathrm{ord}}(\{y_i^{(m)}\}) = 0$; $G^{\mathrm{dis}}(\{x_i\})$ contains all the parameters needed to describe the disordered phase and is given by eq. (1). $\Delta G^{\mathrm{ord}}(\{y_i^{(m)}\})$ is calculated using the sublattices, and one way to ensure that it is zero when the phase is disordered is to calculate eq. (5) twice, once with the original site fractions, $y_i^{(m)}$, and once with them replaced by the mole fractions, x_i, as follows:

$$\Delta G^{\mathrm{ord}} = G^{2\mathrm{sl}}(\{y_i^{(m)}\}) - G^{2\mathrm{sl}}(\{y_i^{(m)} = x_i\}). \quad (7)$$

2.3 Gibbs energy of FCC-based phases with four sublattices

To describe ordered structures in the FCC lattice, the four sublattices were selected in the way that all sublattices were equivalent, had an equal number of sites, and bonds to the other sublattices. The Gibbs energy equation for a four-sublattice phase in an *i-j* binary system using the CEF is:

$$G^{4\mathrm{sl}} = \sum_{i,j,k,l} y_i^{(1)} y_j^{(2)} y_k^{(3)} y_l^{(4)} G_{i:j:k:l} + RT\frac{1}{4}\sum_{m=1}^{4}\sum_{i} y_i^{(m)} \ln y_i^{(m)} \quad (8)$$

where $G_{i:j:k:l}$ is the Gibbs energy of the *i*:*j*:*k*:*l* compound. In this model, as presented in Fig. 1(b), the FCC lattice is divided into four simple cubic sublattices which are equivalent to each other. In the four-sublattice model, the sublattices are numbered as #1, #2, #3, and #4 from left to right in the suffix of the Gibbs energy of the compounds. Therefore, $L1_0$ and $L1_2$ ordered phases are written as #1=#2≠#3=#4 ($L1_0$), and #1=#2=#3≠#4 ($L1_2$). Because of the symmetry of the sublattice configurations, the Gibbs energies of the end members in the *i-j* binary system have to fulfill the relations:

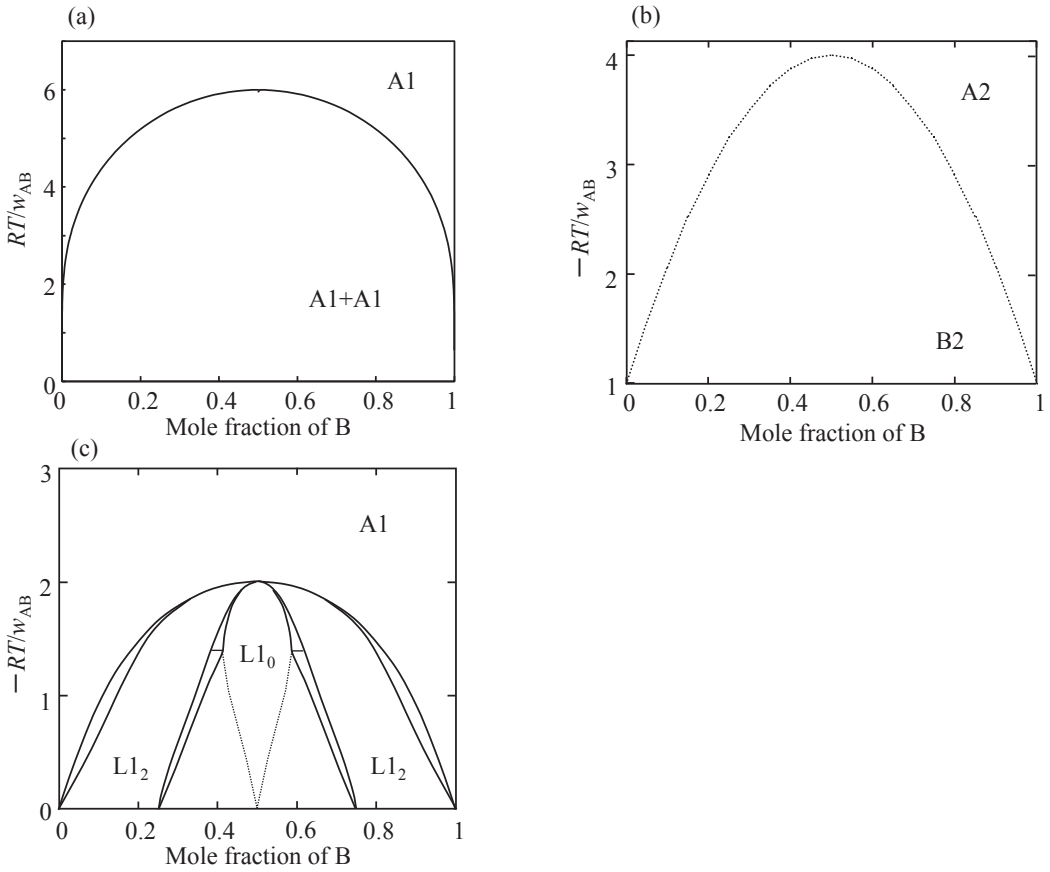

Fig. 2 A-B binary phase diagrams: (a) miscibility gap with the interaction parameter $w_{A,B} = +1\,\mathrm{kJ\,mol^{-1}}$ and the coordination number z = 12, (b) order-disorder transition in the BCC lattice with $w_{A,B} = -1\,\mathrm{kJ\,mol^{-1}}$, and (c) order-disorder transitions in the FCC lattice with $w_{A,B} = -1\,\mathrm{kJ\,mol^{-1}}$. The dotted lines indicate the second-order transitions.

$$\begin{aligned} G_{i:i:i:j} &= G_{i:i:j:i} = G_{i:j:i:i} = G_{j:i:i:i} = 3w_{i,j}, \\ G_{i:i:j:j} &= G_{i:j:i:j} = G_{i:j:j:i} = G_{j:i:i:j} = G_{j:i:j:i} \\ &= G_{j:j:i:i} = 4w_{i,j}, \\ G_{j:j:j:i} &= G_{j:j:i:j} = G_{j:i:j:j} = G_{i:j:j:j} = 3w_{i,j}. \end{aligned} \tag{9}$$

Using the same manner in eq. (9), the constraints due to the symmetry are applied for the *i-j-k* ternary and *i-j-k-l* quaternary end members. They can be given by counting unlike pairs, as

$$\begin{aligned} G_{i:i:j:k} &= 2w_{i,j} + 2w_{i,k} + w_{j,k}, \\ G_{i:j:k:l} &= w_{i,j} + w_{i,k} + w_{i,l} + w_{j,k} + w_{j,l} + w_{k,l}. \end{aligned} \tag{10}$$

The Gibbs energy of FCC phases with four sublattices is given by the CEF using eq. (7), where $\Delta G^{\mathrm{ord}} = G^{4\mathrm{sl}}(\{y_i^{(m)}\}) - G^{4\mathrm{sl}}(\{y_i^{(m)} = x_i\})$.

To calculate the phase equilibria, isothermal sections, and transition temperatures, the Gibbs energy functions were written in a TDB format[17] for Pandat,[18] CaTCalc,[19] and Thermo-Calc[20] software packages used in the present work.

3. Results and Discussions

3.1 Stability range of the single solid-solution phase in binary systems

The A-B binary phase diagrams are calculated using the Gibbs energies defined in Section 2. When the interaction parameter between A and B is repulsive, i.e., $w_{A,B} = +1\,\mathrm{kJ\,mol^{-1}} > 0$, the solid-solution phase decomposes into two phases at low temperatures, as presented in Fig. 2(a). When the interaction parameter between A and B is attractive, i.e., $w_{A,B} = -1\,\mathrm{kJ\,mol^{-1}} < 0$, the long-range orderings take place at low temperatures, as presented in Figs. 2(b) and (c).

For the miscibility gap in the A-B binary system, the peak temperature of the two-phase region can be obtained by putting the second derivative of the Gibbs energy in eq. (1) with respect to the mole fraction to zero,

$$\frac{d^2 G^{\mathrm{dis}}}{dx_{\mathrm{B}}^2} = 0. \tag{11}$$

At the equiatomic composition, the peak temperature T_{C} of the miscibility gap is $+zw_{A,B}/2R$ ($+6w_{A,B}/R$ in the FCC lattice and $+4w_{A,B}/R$ in the BCC lattice). For the order-disorder transition in the A-B binary system, T_{C} can be obtained from the second derivative of the Gibbs energy in eq. (5) for A2/B2 and in eq. (8) for A1/$L1_0$ with respect to the site fraction to zero. The peak temperature of the A2/B2 transition is $-4w_{A,B}/R$ at the equiatomic composition. The A1/$L1_0$ transition at the equiatomic composition is $-2w_{A,B}/R$. Using thermodynamic software packages, these relations were confirmed numerically as presented in Figs. 3(a) and (b).

It should be noted that the purpose of this study is to discuss the relative stability of the disordered state, whereas the thermodynamic modeling of the order-disorder transitions. Based on the B-W-G approximation, it is known that

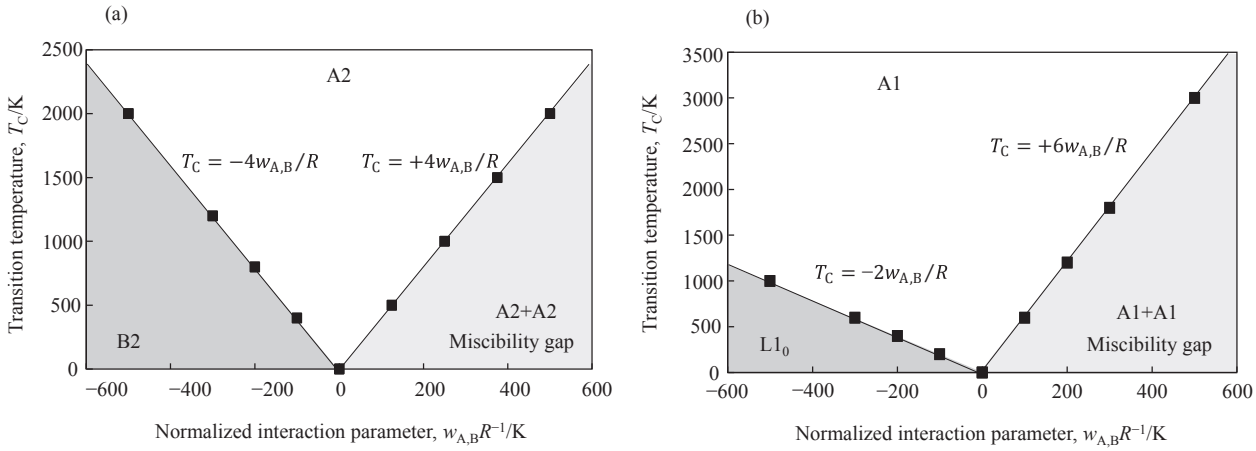

Fig. 3 Calculated transition temperatures, T_C, of the equiatomic alloy in the A-B binary system as a function of the normalized interaction parameter $w_{A,B}R^{-1}$ in the (a) BCC lattice and (b) FCC lattice.

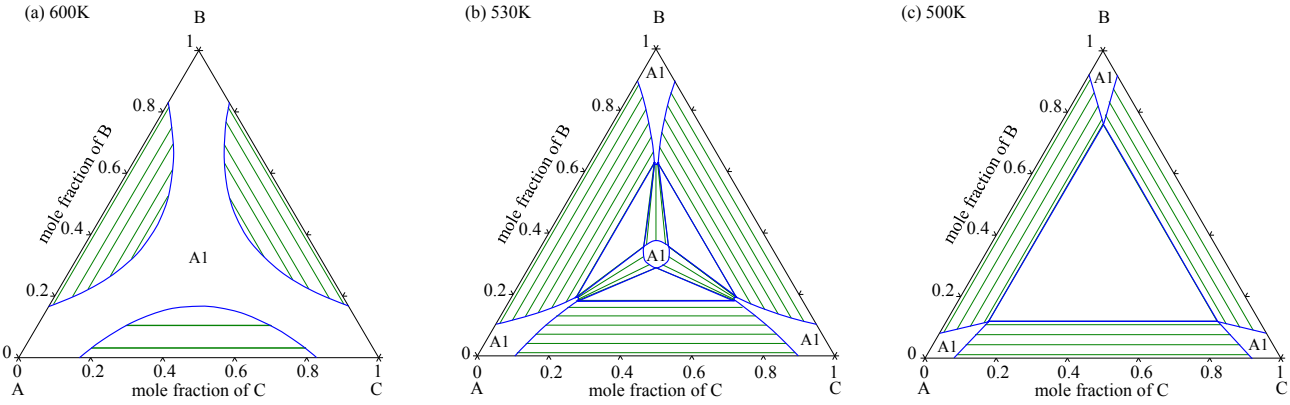

Fig. 4 Isothermal sections with the miscibility gaps in the A-B-C ternary system at (a) 600 K, (b) 530 K, and (c) 500 K. The interaction parameters used in the calculations are $w_{A,B} = w_{A,C} = w_{B,C} = w = 1\,\mathrm{kJ\,mol^{-1}}$. The coordination number is z = 12 (FCC lattice).

the Al/$L1_0$ transition at the equiatomic composition is the second order[21] as presented in Fig. 2(c), while it is the first order transition in the real alloy systems.[22,23] For detailed discussions of the order-disorder transitions, it may require more precise thermodynamic models such as the cluster variation method.

3.2 Stability range of the single solid-solution phase in ternary systems

In this section, the stability of the solid-solution phases is examined in the A-B-C ternary system. The interaction parameters used in the calculations are as follows:

$$w_{A,B} = w_{A,C} = w_{B,C} = w. \tag{12}$$

The isothermal sections of the ternary system were calculated for the FCC lattice, and are presented in Figs. 4(a), (b), and (c). Since the interaction parameter is positive (repulsive between A, B, and C), i.e., $w = +1\,\mathrm{kJ\,mol^{-1}}$, the FCC solid solution has miscibility gaps. At 600 K in Fig. 4(a), there are three two-phase regions. At 500 K in Fig. 4(c), one three-phase triangle appears in the middle of the ternary isotherm and the single solid-solution phase is only stable at the corners of the pure elements. At an intermediate temperature (530 K), the two-phase regions in Fig. 4(a) merge and form three three-phase triangles (Fig. 4(b)). It is worth emphasizing that the single solid-solution region remains around the equiatomic composition. This is because the configurational entropy S^{conf} has the largest value at the equiatomic composition, which stabilizes the solution phase. Detailed examinations of the stability of solution phases to the spinodal decompositions in ternary systems can be found in the literature.[24]

When the interaction parameter is negative in the BCC lattice (attractive between A, B, and C), i.e., $w = -1\,\mathrm{kJ\,mol^{-1}}$, the calculated isothermal sections are presented in Figs. 5(a), (b), and (c). B2-type ordering (#1≠#2) at 500 K occurs around the binary stoichiometric compositions (AB, AC, and BC), as presented in Fig. 5(a). As the temperature decreases to 100 K (Fig. 5(c)), the single solid-solution regions are limited to the corners of pure elements A, B, and C. At an intermediate temperature (350 K) in Fig. 5(b), the single solid-solution region remains as stable around the equiatomic composition.

For the orderings of the FCC lattice in the ternary system, the calculated isothermal sections are presented in Figs. 6(a) and (b), where the interaction parameter $w = -1\,\mathrm{kJ\,mol^{-1}}$ was used for the calculations on CaTCalc software.[18] In binary systems, the A1, $L1_0$, and $L1_2$ phases can be described by equivalence in sublattices such as (1) #1=#2=#3=#4, (2) #1=#2≠#3=#4, and (3) #1=#2=#3≠#4, respectively. The

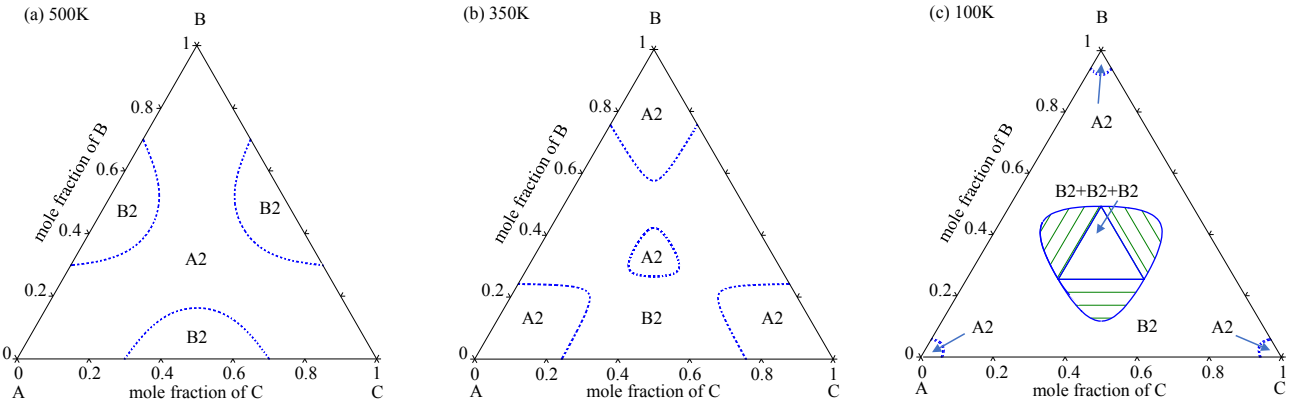

Fig. 5 Isothermal sections with the order-disorder transitions in the A-B-C ternary system at (a) 500 K, (b) 350 K, and (c) 100 K. The interaction parameters used in these calculations are $w_{A,B} = w_{A,C} = w_{B,C} = w = -1\,\mathrm{kJ\,mol^{-1}}$. The dotted lines indicate the second-order transitions.

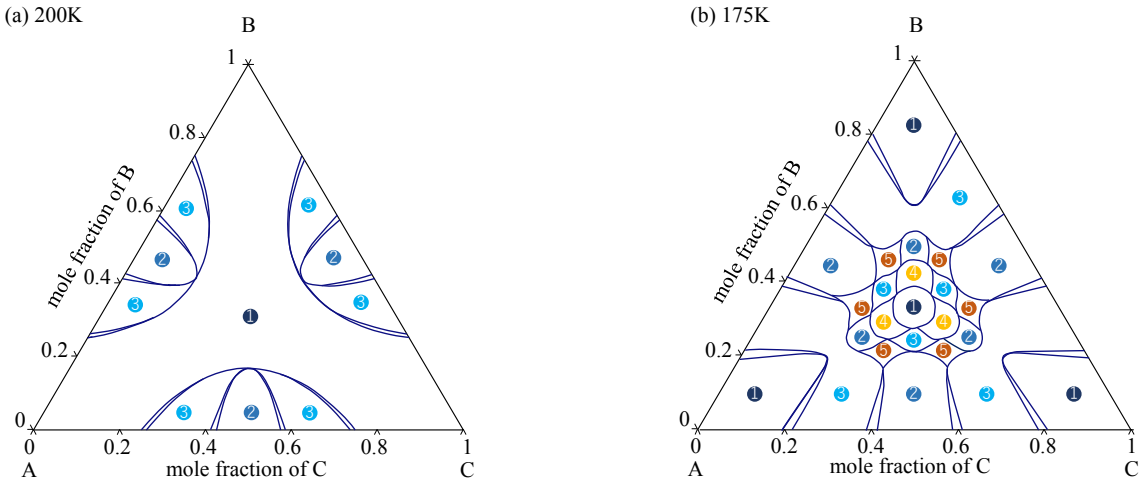

Fig. 6 Isothermal sections with the order-disorder transitions in the FCC lattice with four sublattices at (a) 200 K and (b) 175 K. The interaction parameters used in these calculations are $w_{A,B} = w_{A,C} = w_{B,C} = w = -1\,\mathrm{kJ\,mol^{-1}}$. The numbers in the figures indicate phases; 1: A1 disordered phase (#1=#2=#3=#4), 2: $L1_0$-type ordered phase (#1=#2≠#3=#4), 3: $L1_2$-type ordered phase (#1=#2=#3≠#4), 4: an ordered phase (#1=#2≠#3≠#4), and 5: an ordered phase (#1=#2≠#3≠#4, $y_A^{(3)} = y_C^{(4)}$, $y_C^{(3)} = y_A^{(4)}$, $y_B^{(3)} = y_B^{(4)}$).

ordering behaviors are more complex in the ternary systems, as higher-order phases can be stable in the central part of the isothermal section in Fig. 6(b). The indicated configurations of the ternary ordered phases are (4) #1=#2≠#3≠#4, and (5) #1=#2≠#3≠#4, $y_A^{(3)} = y_C^{(4)}$, $y_C^{(3)} = y_A^{(4)}$, and $y_B^{(3)} = y_B^{(4)}$. In addition, there are two more configurations: (6) #1≠#2≠#3≠#4, and (7) #1≠#2≠#3≠#4, $y_A^{(1)} = y_C^{(2)}$, $y_C^{(1)} = y_A^{(2)}$, $y_B^{(1)} = y_B^{(2)}$, $y_A^{(3)} = y_C^{(4)}$, $y_C^{(3)} = y_A^{(4)}$, and $y_B^{(3)} = y_B^{(4)}$, which are not stable in Fig. 6(b). Consequently, the phase equilibria on the isothermal sections become complex with these ordered phases in the four-sublattice model using the CEF.[25] At low temperatures, where the disordered state is not stable in any of the compositions, an isothermal section cannot be fully calculated with any of the thermodynamic calculation packages adopted in the present work and is hence omitted in Fig. 6.

In this section, the stability of the solid-solution phases was examined in the A-B-C ternary system. The results can be summarized that the single solid-solution phases in all three configurations in Figs. 4–6 become stable around the equiatomic composition, where S^{conf} has the largest value. Consistently, around the equiatomic compositions, HEAs can be effectively synthesized.

3.3 Transition temperature (T_C) in higher-order systems

In Section 3.2, it was demonstrated that the single solid-solution phase became stable around the equiatomic composition in ternary systems in the BCC and FCC lattices. In this section, we investigate the change in the transition temperature of equiatomic alloys with the number of elements in the system. In Figs. 7(a) and (b), the transition temperatures of the equiatomic alloys are numerically calculated using thermodynamic software packages and are presented as a function of the normalized interaction parameter, wR^{-1}. With an increase in the number of elements in the system (n), the transition temperature decreases. The horizontal bars indicate the ranges where the HEAs are observed.[10] Previously reported HEAs were in the range of the single solid-solution phase.

In Fig. 8, the transition temperature is presented as a function of the number of elements in the system, where the interaction parameters are $w = +1\,\mathrm{kJ\,mol^{-1}}$ for the misci-

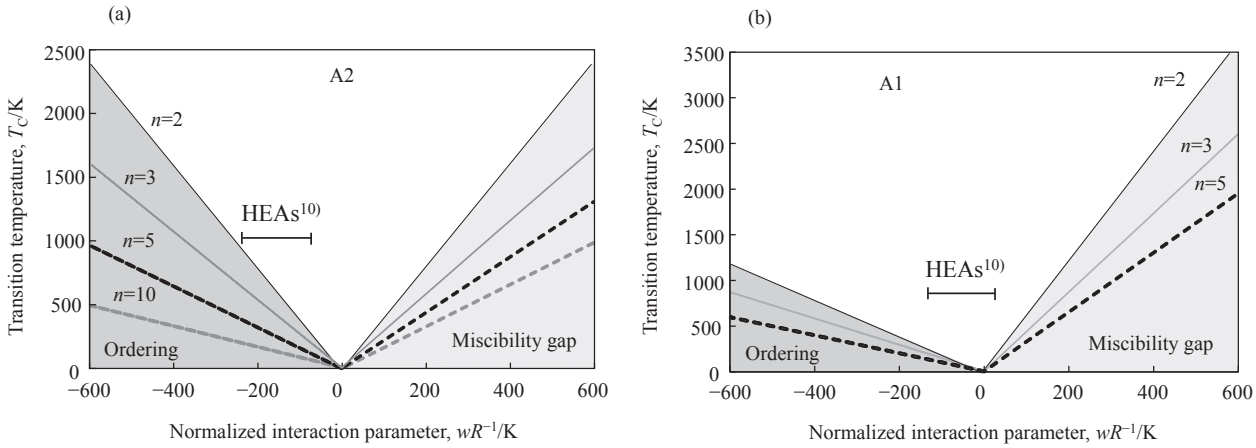

Fig. 7 Calculated transition temperatures, T_C, of the equiatomic alloy in the n-element system as a function of the normalized interaction parameter wR^{-1} in the (a) BCC lattice and (b) FCC lattice. The horizontal bars indicate the range of HEAs, as previously reported.[10)]

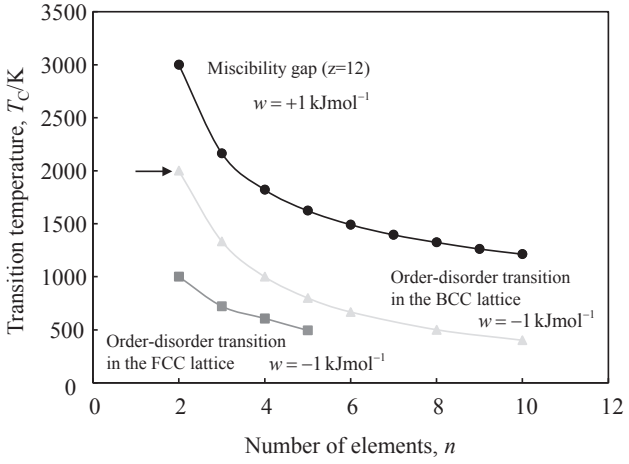

Fig. 8 The calculated transition temperatures, T_C, of the equiatomic alloys as a function of the number of elements in the system, n. The interaction parameters used in the calculations are given in the figure. The arrows indicate the equiatomic alloys where the end member exists in the BCC lattice.

bility gap and $w = -1\,\mathrm{kJ\,mol^{-1}}$ for the orderings in the FCC and BCC lattices. Due to the increase in S^{conf}, the transition temperatures decrease with increasing n in the system. Notably, the order-disorder transition temperature curve does not smoothly decrease with increasing n. This is possibly due to the stoichiometric compositions of the ordered phases at the equiatomic composition, where $A_{0.5}B_{0.5}$ in the A-B binary system ($n = 2$) and $A_{0.25}B_{0.25}C_{0.25}D_{0.25}$ in the A-B-C-D quaternary system ($n = 4$) are in equilibrium with the disordered phase at the transition temperature. Consequently, the transition temperature becomes slightly higher due to the stoichiometry of the compounds in equilibrium with the solution phase. To avoid stoichiometric compounds at the equiatomic composition, adding more than four elements may be effective because quaternary stoichiometric compounds of transition elements are rarely found in Pearson's crystal structure database.[26)] For the A2 and B2 phases described by the CEF with the two sublattices, although the stoichiometric compound is formed at the equiatomic composition in the binary system ($n = 2$, indicated by an arrow in Fig. 8), the curve seems to be smoothly changing. This may suggest that this effect is not significant in the BCC lattice with the present sublattice configurations.

3.4 Variations in the interaction parameters in ternary systems

In the previous sections, the phase equilibria were calculated for the symmetric cases where all the interaction parameters were the same as in eq. (12). However, binary interactions are different in actual multi-component systems. Therefore, in the present section, we examine the change in the transition temperature with small changes in the interaction parameters. When the interaction parameters have the same values, the A1 phase becomes stable at 530 K around the equiatomic composition, as presented in Fig. 4(b). With a weaker repulsive interaction between B and C ($w_{B,C} = +0.9\,\mathrm{kJ\,mol^{-1}}$) than others ($w_{A,B} = w_{A,C} = +1\,\mathrm{kJ\,mol^{-1}}$), the A1 single-phase region at the center of the isothermal section disappears (Fig. 9(a)) and becomes wider. With an even more repulsive interaction ($w_{B,C} = +1.1\,\mathrm{kJ\,mol^{-1}}$) than the others, the single solid-solution phase at the equiatomic composition also disappears, and the three-phase triangle becomes stable (Fig. 9(b)). This is qualitatively the same for the ordering cases, as presented in Figs. 10(a) and (b) for the BCC lattice and Figs. 11(a) and (b) for the FCC lattice. The ordered states are less stable with less attractive $w_{B,C} = -0.9\,\mathrm{kJ\,mol^{-1}}$, and more stable with more attractive $w_{B,C} = -1.1\,\mathrm{kJ\,mol^{-1}}$ interactions, while the other interactions are the same, $w_{A,B} = w_{A,C} = -1\,\mathrm{kJ\,mol^{-1}}$. Because the ordering behaviors are complex in the present four-sublattice model, as mentioned in Section 3.2, thermodynamic calculation packages cannot completely solve isothermal sections at low temperatures. Figure 11(b) is a typical example where the phase equilibria at the central part of the isothermal section are not well calculated. Hence, the stable phases were confirmed based on point calculations on CaTCalc software. The results revealed that the A1 phase was not stable in the central part of the diagram. These slight changes in the interactions between B and C result in different isothermal sections. The change of $\pm 0.1\,\mathrm{kJ\,mol^{-1}}$ in the interaction parameter approximately corresponds to a change of $\pm 2\,\mathrm{kJ\,mol^{-1}}$ in the mixing enthalpy at the

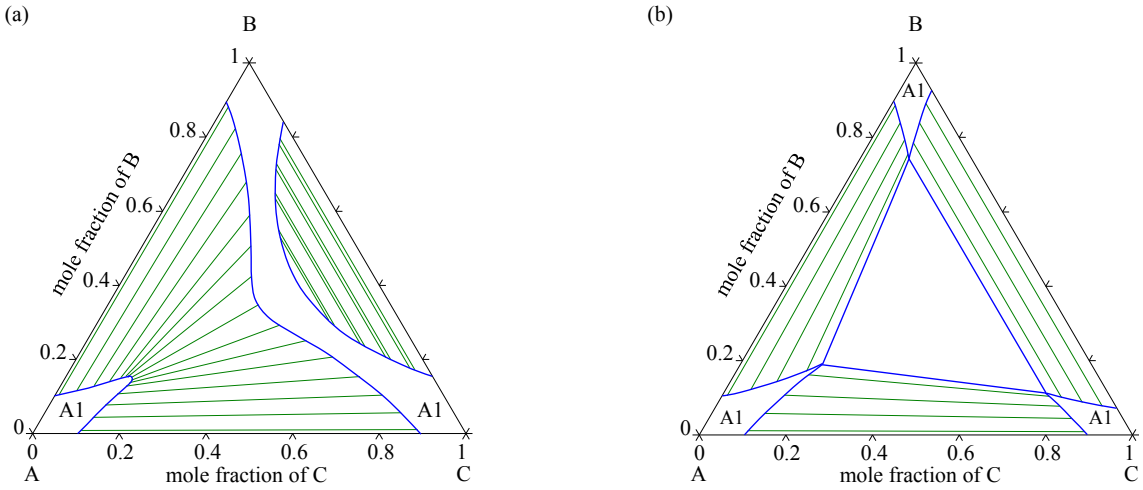

Fig. 9 Miscibility gaps in the FCC lattice at 530 K where the interaction parameters used in the calculations are $w_{A,C} = w_{A,C} = +1$ kJ mol^{-1}, and (a) $w_{B,C} = +0.9$ kJ mol^{-1} and (b) $w_{B,C} = +1$ kJ mol^{-1}.

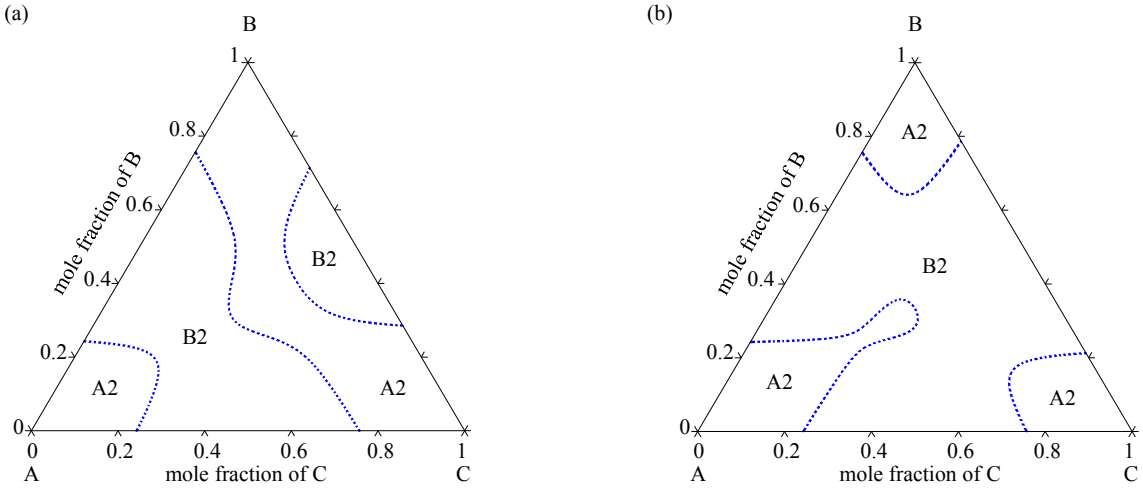

Fig. 10 Order-disorder transitions in the BCC lattice at 350 K, where the interaction parameters used in the calculations are $w_{A,C} = w_{A,C} = -1$ kJ mol^{-1}, and (a) $w_{B,C} = -0.9$ kJ mol^{-1} and (b) $w_{B,C} = -1.1$ kJ mol^{-1}. The dotted lines indicate the second-order transitions.

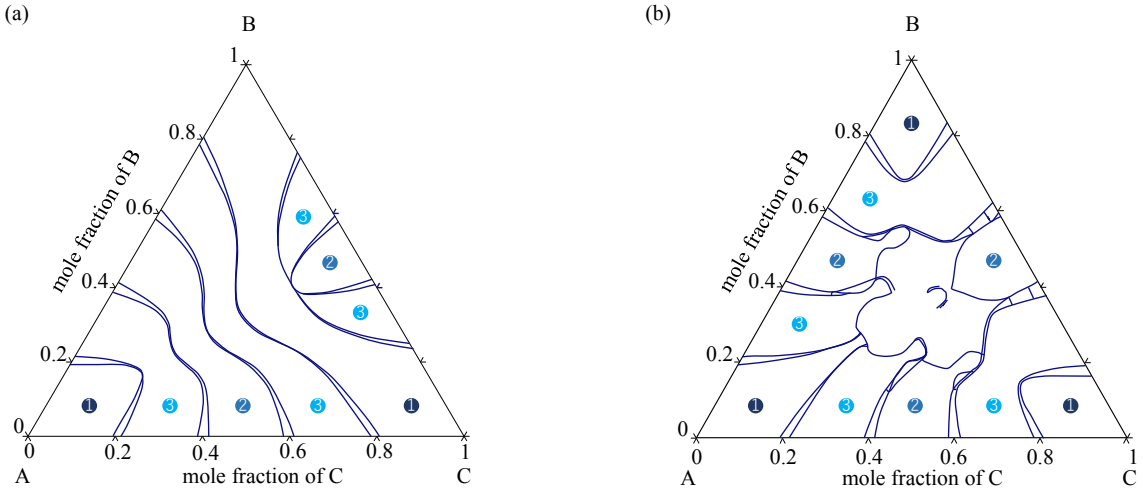

Fig. 11 Order-disorder transitions in the FCC lattice at 175 K where the interaction parameters used in the calculations are $w_{A,C} = w_{A,C} = -1$ kJ mol^{-1}, and (a) $w_{B,C} = -0.9$ kJ mol^{-1} and (b) $w_{B,C} = -1.1$ kJ mol^{-1}. The numbers in the figures indicate the phases; 1: A1 disordered phase (#1=#2=#3=#4), 2: $L1_0$-type ordered phase (#1=#2≠#3=#4), and 3: $L1_2$-type ordered phase (#1=#2=#3≠#4). The phase areas in the central part are not resolved since the calculation is not completed.

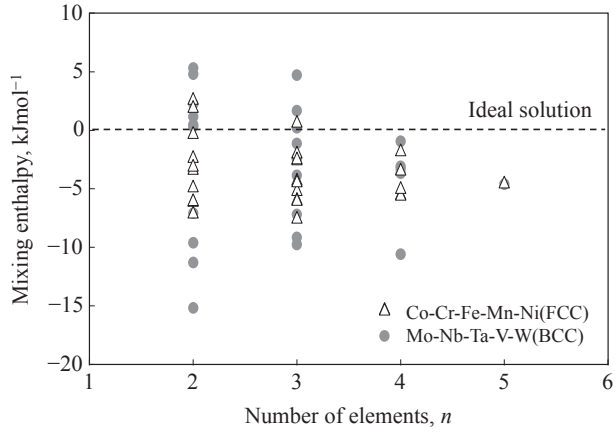

Fig. 12 Mixing enthalpy of equiatomic alloys in n-element systems in the FCC- and BCC-based HEAs.

equiatomic composition. With this variation, the stability of the solid-solution phase is affected and can decrease. This variation is smaller than the variations in the mixing enthalpy in the binary subsystems of the Cantor alloy,[27] where they are in the range of $+3\sim-7\,\mathrm{kJ\,mol^{-1}}$. This contradicts the fact that Cantor alloys and many HEAs have been synthesized.[10] One of the reasons is that the mixing enthalpies of equiatomic alloys converge to an ideal solution with the increasing number of elements in the system. The convergence in the Cantor alloy and the BCC-based HEA is demonstrated in Fig. 12.[27–29] This implies that the characteristics of the binary interactions are averaged in multi-component systems. Consequently, HEAs can accommodate a variety of elements with different interaction parameters.

4. Conclusions

In the present study, using the regular solution model and CEF with two and four sublattices, the stability of the solid-solution phases was examined in multi-component alloys based on the CALPHAD technique. The following results were obtained:

(1) The isothermal sections of the ternary systems with miscibility gaps and orderings on the BCC and FCC lattices were calculated using the thermodynamic models. The results exhibited that the single solid-solution region remained stable around the equiatomic composition, where S^{conf} had the largest value in the system.

(2) The transition temperatures from the disordered state to the ordered state or miscibility gaps decreased with the increasing number of elements in the system. The order-disorder transition temperature in the FCC lattice was affected by the end member of the ordered phase existing at the equiatomic composition, whereas it was not significant for the order-disorder transition in the BCC lattice.

(3) The stability of the single solid-solution phases at equiatomic compositions was affected by small variations in the interaction parameters. By adding multiple elements, the characteristics of the binary interactions were averaged; this resulted in HEAs comprising a variety of elements whose interaction parameters were different.

Acknowledgments

This work was supported by the Grant-in-Aid for Scientific Research on Innovative Area, “High Entropy Alloys” (No. 18H05454).

REFERENCES

1) J.-W. Yeh, S.-K. Chen, S.-J. Lin, J.-Y. Gan, T.-S. Chin, T.-T. Shun, C.-H. Tsau and S.-Y. Chang: Adv. Eng. Mater. **6** (2004) 299–303.
2) B. Cantor, I.T.H. Chang, P. Knight and A.J.B. Vincent: Mater. Sci. Eng. A **375–377** (2004) 213–218.
3) J.-I. Lee, K. Tsuchiya, W. Tasaki, H.-S. Oh, T. Sawaguchi, H. Murakami, T. Hiroto, Y. Matsushita and E.-S. Park: Sci. Rep. **9** (2019) 13140.
4) M. Kawamura, M. Asakura, N.L. Okamoto, K. Kishida, H. Inui and E.P. George: Acta Mater. **203** (2021) 116454.
5) D. Zhou, Z. Chen, K. Ehara, K. Nitsu, K. Tanaka and H. Inui: Scr. Mater. **191** (2021) 173–178.
6) O.N. Senkov, D.B. Miracle, K.J. Chaput and J.-P. Couzinie: J. Mater. Res. **33** (2018) 3092–3128.
7) V. Soni, B. Gwalani, O.N. Senkov, B. Viswanathan, T. Alam, D.B. Miracle and R. Banerjee: J. Mater. Res. **33** (2018) 3235–3246.
8) A. Takeuchi, T. Wada and H. Kato: Mater. Trans. **60** (2019) 2267–2276.
9) K. Enoki and H. Ohtani: Proc. Fall. Meetings Japan Inst. Metals Mater., S3.23 (2020).
10) X. Yang and Y. Zhang: Mater. Chem. Phys. **132** (2012) 233–238.
11) A. Takeuchi: Mater. Trans. **61** (2020) 1717–1726.
12) A. Takeuchi, K. Yubuta and T. Wada: Mater. Trans. **60** (2019) 330–337.
13) A. Takeuchi, T. Wada, T. Nagase and K. Amiya: Mater. Trans. **63** (2022) 835–844.
14) H.L. Lukas, S.G. Fries and B. Sundman: *Computational Thermodynamics*, (Cambridge, 2007).
15) T. Abe, K. Ogawa and K. Hashimoto: Calphad **38** (2012) 161–167.
16) M. Hillert: J. Alloy. Compd. **320** (2001) 161–176.
17) T. Abe: *Thermodynamic Calculations Based on the CALPHAD Technique*, (Uchida Rokakuho, Tokyo, 2011).
18) PANDAT, CompuTherm LLC, 2023.1.10, http://www.computherm.com/.
19) CaTCalc, Res. Inst. of Computational Thermodynamics, 2023.1.10, https://en.rictsystems.com/software.
20) Thermo-Calc, Thermo-Calc Software, 2023.1.10, http://www.thermocalc.com/.
21) T. Mohri: Materia Japan **61** (2022) 265–274.
22) B. Sundman, D.G. Fries and W.A. Oates: Calphad **22** (1998) 335–354.
23) X.-G. Lu, B. Sundman and J. Ågren: Calphad **33** (2009) 450–456.
24) J.E. Morral and S. Chen: J. Phase Equilibria Diffus. **42** (2021) 673–695.
25) A. Kusoffsky, N. Dupin and B. Sundman: Calphad **25** (2001) 549–565.
26) P. Villars and K. Cenzual: *Pearson's Crystal Data: Crystal Structure Database for Inorganic Compounds*, (ASM International, Ohio, 2022).
27) T. Abe: Mater. Trans. **61** (2020) 610–615.
28) T. Abe: Mater. Trans. **62** (2021) 711–718.
29) Computational phase diagram database, NIMS, 2023.1.10, https://mits.nims.go.jp/en/.